# Enthalpy-based Thermal Evolution of Loops: III. Comparison of zero-dimensional models

P. J. Cargill[1,2], S.J. Bradshaw[3] and J.A. Klimchuk[4]

1. Space and Atmospheric Physics, The Blackett Laboratory, Imperial College, London SW7 2BW
2. School of Mathematics and Statistics, University of St Andrews, St Andrews, Scotland KY16 9SS
3. Department of Physics and Astronomy, Rice University, Houston, TX 77005
4. NASA Goddard Space Flight Center, Solar Physics Lab., Code 671, Greenbelt, MD 20771

## Abstract

Zero dimensional (0D) hydrodynamic models, provide a simple and quick way to study the thermal evolution of coronal loops subjected to time-dependent heating. This paper presents a comparison of a number of 0D models that have been published in the past and is intended to provide a guide for those interested in either using the old models or developing new ones. The principal difference between the models is the way the exchange of mass and energy between corona, transition region and chromosphere is treated, as plasma cycles into and out of a loop during a heating-cooling cycle. It is shown that models based on the principles of mass and energy conservation can give satisfactory results at some, or, in the case of the Enthalpy Based Thermal Evolution of Loops (EBTEL) model, all stages of the loop evolution. Empirical models can lead to low coronal densities, spurious delays between the peak density and temperature, and, for short heating pulses, overly short loop lifetimes.

Submitted: 17 June 2012.

## 1. Introduction

Modelling the response of coronal loops to time-dependent flare or flare-like heating has a long history (e.g. Peres, 2000). The most common approach is to study the plasma behaviour along a magnetic field line (or flux bundle, or strand, or loop) with a one dimensional (1D) hydrodynamic (hydro) code (e.g. Mariska et al., 1982; Pallavicini et al., 1983; McClymont and Canfield, 1983; Klimchuk et al., 1987; Hansteen, 1993; Bradshaw and Mason, 2003). This has led to a good generic understanding of how the loop fills with plasma in response to heating, and how, once the heating ceases, the corona drains.

While 1D hydro codes provide a point by point description of a loop's evolution, there are drawbacks, the most serious being the restriction imposed on the timestep due to thermal conduction in the transition region, especially in tenuous loops, and the treatment of chromospheric radiation (see Introduction of Paper 2). As 1D codes become more complicated, with adaptive grids and the tracking of multiple ionisation states, considerable expertise is needed to run them and interpret their output. Thus workers interested in a quick estimate of loop evolution may not have the time, inclination, or expertise to carry out a 1D hydro simulation and there is a need for hydro models that can be run quickly and interpreted easily. This led to the development of zero-dimensional (0D) models which deal with plasma quantities that are either averaged over a loop, or evaluated at a specific point, such as the apex.

The key to the success of a 0D model is the understanding of the exchange of material between the hot corona and cooler transition region (TR) and chromosphere, as discussed in Section 2. We have recently developed a 0D model that we believe addresses this problem in a realistic way (Klimchuk et al., 2008; Cargill et al., 2012, hereafter Papers 1 and 2 respectively). In the course of this work, we found it useful to compare and contrast our approach with other 0D models developed over the past three decades, and a brief initial assessment of this appeared in Section 5 of Paper 1.

The purpose of this paper is to carry out a full comparison of 0D models by solving identical problems with various models. The motivation is as follows: (i) by analysing the assumptions used in each model, and their successes and failures, one can identify

the essential physics in loop evolution. (ii) For workers interested in running 0D models, it is useful to have an assessment of how each approach performs on a specific problem and (iii) the paper aims to help those who wish to develop future 0D models avoid pitfalls. This paper is not intended to be overly critical of older models, which in some cases introduced new ways of approaching 0D modelling, and also contain enlightening discussion. Rather it should be viewed in the spirit of how the assumptions implemented in the past can used to build better 0D models.

Section 2 provides an overview of the basic formulation of 0D models. Several models are examined, as proposed by Kuin and Martens (1982: KM82), Fisher and Hawley (1990: FH90), Kopp and Poletto (1993: KP93), Cargill (1994: C94), Klimchuk et al (2008) and Cargill et al (2012: EBTEL), Aschwanden and Tsiklauri (2009: AT09), and are described in Section 3 and Appendices A and B. Section 4 presents extensive results for the models and compares them with results from the 1D hydro Hydrad code (Bradshaw and Mason, 2003; Bradshaw and Cargill, 2006).

## 2. 0D Models: Introduction

The response of loop plasma to a short burst of heating is well known, and follows three phases. (i) During the initial heating, the temperature rises, but is limited by thermal conduction. The TR and upper chromosphere are unable to radiate away the downward heat flux, so material there is heated and moves into the corona ("evaporation": Antiochos and Sturrock, 1978). (ii) As the heating diminishes, the temperature decreases from its maximum value. The TR can now radiate away more of the heat flux since its density is higher, so that the upflow decreases. In this phase, the increasing coronal density makes radiation more important, and eventually coronal radiative losses exceed those due to conduction. The peak coronal density corresponds approximately to the transition between conductive-dominated and radiative-dominated cooling (e.g. Cargill, 1994, Cargill et al., 1995). (iii) As the loop continues to cool, the heat flux is now too small to power the TR radiation. Instead, a downward enthalpy flux is established, and the corona is drained (Antiochos, 1980; Serio et al., 1991; Bradshaw and Cargill, 2010a,b). In a 1D model, this sequence of events can be followed easily, provided the transition region is resolved adequately

and there is a large enough mass reservoir in the initial upper chromosphere. It is this sequence of events that a 0D model must address.

The evolution of a loop of half-length $L$ is described by the 1D equations of mass, momentum and energy conservation along a field line:

$$\frac{\partial n}{\partial t} + \frac{\partial}{\partial s}(nv) = 0 \tag{1}$$

$$\frac{\partial p}{\partial s} = -m_i n g_{\parallel} \tag{2}$$

$$\frac{\partial E}{\partial t} = -\frac{\partial}{\partial s} v(E + p) - \frac{\partial F_c}{\partial s} + Q - n^2 \Lambda(T) \tag{3}$$

where $v$ is the velocity, $E = p/(\gamma - 1)$, $F_c = -\kappa_0 T^{5/2}(\partial T / \partial s)$ is the heat flux, $Q(s,t)$ is a heating function that includes both steady and time-dependent components, $\Lambda(T) = \chi T^{\alpha}$ is the radiative loss function in an optically thin plasma, and $s$ is the spatial coordinate along the magnetic field. There is also an equation of state: $p = 2nkT$. Subsonic flows are assumed in all the 0D models discussed here, so the terms proportional to $V^2$ or higher are already neglected in Eq (2) and (3).

There are two approaches to 0D modelling. One solves Eq (1) – (3) by integrating over the loop (or part of the loop) to construct a solution for either average or apex quantities (KM82, KP93, EBTEL). The second splits the evolution into distinct temporal phases in which different physical processes dominate, that are then joined together (FH90, C94, AT09) to form a piecewise continuous solution. This second approach does not preclude use of the integrated method in some (or all) phases.

To outline the former approach, we integrate Eq (1) and (3) from the loop apex down to an arbitrary position, assumed to be approximately the loop length (Papers 1 and 2), and denoted by subscript "0":

$$\frac{d\bar{n}}{dt} + \frac{(nv)_0}{L} = 0 \tag{4}$$

$$\frac{1}{\gamma - 1}\frac{d\bar{p}}{dt} = -\frac{1}{L}\left(\frac{\gamma}{\gamma - 1} pv + F_c\right)_0 + \bar{Q} - \frac{R_c}{L} \tag{5}$$

Here "overbar" denotes an averaged quantity, $R_c \approx \bar{n}^2 \Lambda(\bar{T})L$ is the total radiative loss between the apex and the level "0", and the enthalpy and heat fluxes are evaluated at level "0". Symmetry is assumed around the loop apex. [We have not made use of Eq (2) since the pressure is defined as a coronal average. Gravitational effects enter when we include the atmosphere below the "0" level.] Below the level "0" is a plasma layer (the TR) that responds to the downward heat or enthalpy flux. While Eq (4) and (5) are widely used in 0D modelling, it is the essential treatment of this lower layer that distinguishes the models. Finally while these equations are written in terms of coronal averages, most workers use apex values as their variables, and so apex values will be our primary variables.

## 3. The Models summarised

We examine the models as originally documented in the literature, unless noted otherwise. There are difficulties in comparing heating functions. In some cases this is because the model can only accommodate one type (in our view a significant drawback), while in others there are restrictions imposed on the temporal form of the heating. This means that it is not possible to compare all models on the same problem.

We now summarise the important points of the models, with the extensive details of FH90 and AT09 in Appendices A and B. Table 1 summarises the capabilities of the models (see caption for full details). The list of criteria is by no means complete, but does contain a number of things that are reasonable to require of a 0D model. In many cases there are caveats, as noted, concerning whether a model does something adequately or not. We return to Table 1 in Section 5.4.

### 3.1 Klimchuk et al (2008), Cargill et al (2012)

Full details of the "The Enthalpy Based Thermal Evolution of Loops" (EBTEL) model can be found in Papers 1 and 2. In EBTEL the region below "0" is the TR that is coupled to the corona through the heat and enthalpy fluxes. Integrating Eq (3) from the chromosphere to level "0", we obtain the TR equation:

$$\frac{\gamma}{\gamma-1}\left(pv+F_c\right)_0+R_{tr}=0 \tag{6}$$

where $R_{tr}$ is the radiative loss integrated over the TR, and the TR thickness is much less than the corona. Both the heat flux and temperature at the TR lower boundary are assumed to be small. Eq (6) says that the incoming heat flux and incoming or outgoing enthalpy flux must adjust to account for the TR radiation. We can combine Eq (6) with (5) to give a coronal equation:

$$\frac{1}{\gamma-1}\frac{d\overline{p}}{dt}=\overline{Q}-\frac{1}{L}\left(R_C+R_{tr}\right) \tag{7}$$

Thermal conduction and enthalpy do not appear in (7) because they involve energy redistribution within the corona/TR system as opposed to a net energy loss. The coronal density comes from (4) in the form:

$$\frac{d\overline{n}}{dt}=\frac{(nv)_0}{L}=-\frac{\gamma-1}{2kT_0L\gamma}\left(F_{c0}+R_{tr}\right). \tag{8}$$

and the coronal temperature is determined by:

$$\frac{1}{\overline{T}}\frac{d\overline{T}}{dt}=\frac{1}{\overline{p}}\frac{d\overline{p}}{dt}-\frac{1}{\overline{n}}\frac{d\overline{n}}{dt} \tag{9}$$

The quantities $R_{tr}$, $T_0$ and $F_{c0}=-(2/7)\kappa_0 T_a^{7/2}/L$, where $T_a$ is the apex temperature of the loop, are defined in terms of coronal averages through three parameters: $C_1=R_{tr}/R_c$, $C_2=\overline{T}/T_a$ and $C_3=T_0/T_a$. $C_2$ and $C_3$ can be taken as constant, with values of 0.9 and 0.6 respectively (Paper 2, Appendix). $C_1$ is, in the absence of gravity, 2 for equilibrium, static loops and 0.6 during radiative cooling. In Paper 2 we discuss the full implementation of $C_1 = C_1(T_a, L)$, in particular how it can model stratification. The static initial conditions require a background heating function and are found by setting the time derivatives zero in Eq (7-9).

### 3.2 Kuin and Martens (1982).

We do not analyse KM82 in depth, but it merits mention as the first attempt to address in a simple fashion the coupling between corona, TR and chromosphere. The domain of integration in Eq (5) was extended to the chromosphere. A lower atmosphere was not included, but the exchange of material through the base was treated as:

$$\frac{dn}{dt} = \frac{(\gamma-1)}{kT}\frac{f\kappa_0 T_i^{5/2}(T-T_i)}{L^2} = \frac{(nv)_0}{L}, \qquad (10)$$
$$0 \le f \le 1 \text{ for } T > T_i, \quad f = 1 \text{ for } T < T_i,$$

where $T_i$ is defined as an "inflection temperature", when conduction changes from a loss to a gain, calculated for static equilibrium. The right hand side of (10) gives the correct direction of the flow for loops that are hotter (upflow) and cooler (downflow) than in equilibrium. Comparing (10) with the corresponding EBTEL equation, TR radiation is not included explicitly, though it is included implicitly for $f < 1$ during evaporative cooling. For $T < T_i$, enthalpy cooling of the corona is not considered.

### 3.3. Kopp and Poletto (1993)

KP93 use equation (5) but with $F_{c0} = -(4/7)\kappa_0 T_a^{7/2}/L$ and $Q = Q_b + Q_i$ includes both background (*b*) and impulsive (*i*) heating terms. [Note the factor 4/7 in the conduction term compared with 2/7 in EBTEL. Since the temperature in the heating phase is determined approximately by a balance between conduction and heating, the difference in the maximum temperature will be of order $2^{2/7} = 1.22$.]

KP93 model the lower atmosphere in a similar generic way to EBTEL. They include an evaporative upflow:

$$v_{ev} = -\frac{\gamma-1}{\gamma}\frac{F_{c0} - F_{c0}(t=0)}{\bar{p}} \qquad (11)$$

where $F_{c0}(t=0)$ is the initial heat flux. Eq (11) always gives an upflow when the heat flux exceeds its initial value. Contrasting this with the relevant equation in EBTEL, (11) fixes the TR radiation at the pre-heating value ($F_{c0}(t=0) \sim R_{tr}(t=0)$). However, as a loop evolves during a heating event, $R_{tr}$ increases, and eventually exceeds the downward heat flux. At this point a downward enthalpy flux is required to power the radiation. Eq (11) does not have such a flow and instead KP93 model loop draining by including a term $v_d = -(1-\bar{n}_0/\bar{n})v_{ff}$, and set $v = v_{ev} + v_d$ in (5). Here $v_{ff} = (2gh)^{1/2}$, $h = 2L/\pi$ is the height of the apex of a semi-circular loop and $\bar{n}_0$ is the average initial loop density. This draining leads to problems with the density, as we shall see.

KP93 define an initial state: $Q_b L = R_{c0} - F_{c0}$, and rewrite Eq (5) in the simple form:

$$\frac{L}{\gamma-1}\frac{d\overline{p}}{dt}=\frac{\gamma}{\gamma-1}\overline{p}v_d+L\overline{Q_i}-\left(R_c-R_{c0}\right) \tag{12}$$

We have coded up the KP93 method, compared this with Figures 1 - 3 of their paper, and are satisfied with the agreement.

### 3.4 Cargill (1994)

We now turn to the second class of models, namely those that split up the coronal evolution into separate phases. C94 assumes that the heating phase is instantaneous (faster than the initial cooling time) and the cooling takes place in two phases. First, the loop cools by conductive evaporation at constant pressure according to Antiochos and Sturrock (1978) and, when the conductive and radiative cooling times are equal, the cooling changes to radiative domination where temperature and density satisfy the scaling $T \sim n^2$ (e.g. Serio et al., 1991; Cargill et al., 1995):

$$T(t)=T_0\left(1+\frac{t}{\tau_{c0}}\right)^{-2/7},\ \frac{n(t)}{n_0}=\frac{T_0}{T(t)},\ \tau_c<\tau_R \tag{13}$$

$$T(t)=T_*\left(1-\frac{3}{2}\left(\frac{1}{2}-\alpha\right)\frac{(t-t_*)}{\tau_{R*}}\right)^{1/(1/2-\alpha)},\ \frac{n(t)}{n_0}=\sqrt{\frac{T(t)}{T_0}},\ \tau_c>\tau_R \tag{14}$$

where $T$ and $n$ are apex values, $\tau_c$ and $\tau_R$ the instantaneous conductive and radiative cooling times, $T_0$ and $n_0$ the temperature and density on cessation of the heating, given by Eq (14) – (16) of Cargill (1994), $\tau_{c0}$ the conductive cooling time at the end of the heating, $t_*$ the time when $\tau_c = \tau_R$ and $\tau_{R*}$ the radiative cooling time at $t = t_*$.

Eq (13) can be derived from (5) by assuming that the coronal pressure remains constant, there is no coronal heating or radiation and the downward heat flux leads only to an upward enthalpy flux. Eq (14) is a semi-empirical result that has not as yet been derived from the basic equations.

### 3.5 Fisher and Hawley (1990)

FH90 introduced some ideas used by later authors, and is discussed fully in Appendix A. They work in terms of the column density: $N=\int n ds$, though recovering the

average and apex density is straightforward. The loop evolution is split into three parts: an initial evaporative phase where heating roughly balances conduction, a phase close to equilibrium, and then a strongly condensing (radiative) phase. It is possible to go from the first to the third phase, with conduction-driven evaporation in the absence of heating not being modelled. FH90 assume that during all stages the column density and pressure are related by a relationship: $N \sim p^{\Omega}$ or, on writing $N$ in terms of an average density $n$ and loop length $L$ as $N \sim nL$, $n \sim p^{\Omega}$. They calculate the index $\Omega$, as described in Appendix A, and then solve the equations of mass and energy conservation. For comparison with EBTEL, we replace the radiative loss function in FH90 by $\Lambda(T) = 1.95\ 10^{-18} T^{-2/3}$

### 3.6 Aschwanden and Tsiklauri (2009)

AT09 present a model that relies largely (though not entirely) on empirical specifications of the temperature and density, and is described fully in Appendix B. A temporal Gaussian heating pulse is used. They split the evolution into three parts: the first up to the time of maximum temperature, $t = t_m$, during which heating and conduction balance, the next to the time of maximum density at $t = t_p$ and a final cooling stage that has some similarity to the familiar $T \sim n^2$ cooling. The second stage is less clear and relies largely on simulation results presented in Tsiklauri et al (2004: hereafter T04), with prescribed ratios of the maximum temperature to the temperature at maximum density and vice-versa, as well as the delay between maximum temperature and maximum density.

## 4. Comparison of Models

### 4.1 Comparison basis

As noted earlier, 0D models can describe a loop using quantities evaluated at the loop apex, or by averages over either the entire loop or just the coronal portion. KP93 use both apex and average quantities in their formalism, but assume them to be approximately equal. C94 used apex values only. EBTEL has simple relations between apex and average values (Paper 2), with the latter being the primary

variables. FH90 treat the apex temperature as a primary variable, and define relations between the total loop column density and the apex density. Since the pressure is spatially constant, one can then work out an average density and temperature. AT09 take apex values as their primary variable, but average temperatures can be calculated.

The relationship between average and apex values is not the same in each model due to different averaging domains. For example, EBTEL has $\bar{T} = 0.9T_a$. FH90 have $\bar{T} = 0.74T_a$ or $0.77T_a$ depending on the phase of evolution. AT09 have $\bar{T} = 0.86T_a$ for uniform heating. Both FH90 and AT09 are averages over the whole loop, so that when the integration is over just the coronal portion, $\bar{T}/T_a$ will increase. If the TR is 10 (20)% of the length, FH90 get $\bar{T} = 0.8\,(0.85)\,T_a$ and AT09 $\bar{T} = 0.9\,(0.93)\,T_a$. To avoid concerns about spatial averaging, we compare EBTEL and Hydrad with the primary variables of the other models, which are usually apex quantities. The comparison between EBTEL and the 1D Hydrad code (Bradshaw and Mason, 2003, Bradshaw and Cargill, 2006) has been discussed extensively in paper 2. However, we include Hydrad runs in several of the cases discussed below.

**4.2 Loop cooling model: C94**

As the first example, we consider the cooling of a hot loop. FH90 and AT09 are excluded because the former cannot model evaporative cooling and the latter requires a heating function. The loop has a half-length of 25 Mm and initial apex temperature and density of 10 MK and $10^9$ $cm^{-3}$ respectively. In all the models discussed, the initial conditions of an equilibrium loop are suspended to accommodate these values.

Figure 1 shows the apex temperature, density and pressure for C94, KP93, EBTEL and Hydrad (dotted, dashed, solid and thick solid lines respectively), and the instantaneous conductive and radiative cooling times for the first three. The Hydrad temperature and pressure fall somewhat faster than EBTEL, while the densities compare well, in line with Paper 2. Looking at KP93, the density and pressure are much lower after 200 secs, the peak density is too small and occurs too soon. The cooling times show that the transition from conductive to radiative cooling in EBTEL corresponds to the time of maximum density, while in KP93 it occurs much later.

We have modified the two models to see when they agree, and conclude that the loop draining model in KP93 is the major cause of the discrepancy. In early cooling, the draining offsets conduction-driven evaporation, and later on inhibits draining as the loop density approaches its initial value. Plasma draining from a hot loop is not due to free-fall motion, but to a downward enthalpy flux required to power the TR radiation during radiative cooling (Bradshaw and Cargill, 2010a,b) and is driven by a mild deviation from hydrostatic equilibrium. Free-fall motions are important in the final loop emptying at low temperatures. Setting $v_d = 0$ in KP93 leads to better agreement with EBTEL. The KP93 density is then larger in the conductive phase, and when we change the value of the conduction coefficient in KP93 to 2/7, and set $C_1 << 1$ in EBTEL, the two agree. So the neglect of TR radiation in KP93 is also significant.

Comparing EBTEL with C94, there is a discrepancy in the timing and value of the maximum density but in both models this occurs when the conductive and radiative cooling times are equal. We find that turning the radiation off at all times in EBTEL gives better agreement with C94 during the conductive cooling phase, though EBTEL has higher temperatures and lower densities due to slightly different conduction coefficients. Turning on only coronal radiation in EBTEL ($C_1 << 1$), reduces the coronal density, with the transition to radiative cooling at around 1600 secs, closer to C94. So it is neither the assumption of separate conduction and (coronal) radiation phases, nor the value of the conduction coefficients, that leads to C94 having a different density. Rather inclusion of the transition region radiation is essential, even at a time when conduction is the more significant coronal loss. In C94 the downward heat flux only drives an upward enthalpy flux, while in EBTEL some of this flux is radiated away as seen in the pressure plot where EBTEL shows energy loss at all times. However, the loop cooling time, defined as the time taken to cool to 1 MK, is similar. Indeed C94 suggested that neglecting radiation during the conduction phase and vice-versa is self-compensating, at least when calculating total cooling times.

### 4.3 Nanoflares: square & triangular heating pulse: FH90, KP93

We next compare FH90, KP93 and EBTEL for nanoflare heating using square and triangular heating pulses. The former was used in FH90 and KP93, and the latter in

EBTEL. Figure 2 shows three cases for square pulses: from top to bottom, case (a) a short (200 sec) and case (b) a long (500 sec) heating pulse in a loop with half-length 25 Mm, and case (c) a long pulse (500 sec) in a loop with L = 75 Mm. The upper and lower panels of Figure 3 shows two cases for a triangular pulse with the same parameters as Figure 2, examples (a) and (c). The pre-heating apex temperature and density are $9\ 10^5$ K and $1.4\ 10^8$ $cm^{-3}$. The heating is turned on abruptly after 100 secs and the maximum heating amplitude for the square (triangular) pulse is $5\ 10^{-3}$ ($10^{-2}$) ergs $cm^{-3}$ $s^{-1}$, so that the total energy injected is the same for both profiles. The three columns in Figures 2 and 3 show the apex temperature, density and pressure as a function of time with solid (EBTEL), dotted (KP93), dashed (FH90) and thick solid lines (Hydrad). The thick dotted lines are described below. AT09 can use only a Gaussian pulse. Hydrad is only shown in the top panels.

Looking first at the KP93 results, the temperature in the initial heating phase agrees well with EBTEL since the physics in both models is similar. However, the density and pressure from KP93 do not compare favourably. The reasons are described in Section 4.2, with the gravitational draining leading to premature termination of the evaporative phase. [We have run KP93 without the draining term and find the density at 800 secs slightly larger than that given by EBTEL.] Figure 3 shows that the problems with KP93 persist for a triangular heating pulse.

We next compare FH90 and EBTEL. The thick dotted lines in the density and pressure plots are EBTEL results with gravity turned off and a single power law loss function. The temperature with these modifications is not shown since the full EBTEL results differ little from the modified ones. The relevant comparison of FH90 is with these modified results. The most important thing to note is the behaviour of the density upon termination of the heating. At that time the density in FH90 begins to fall because evaporation in the absence of heating is not included. On the other hand EBTEL shows the expected conduction-driven evaporation persisting after the termination of heating. This leads to an under-estimation of density in FH90, and an earlier density maximum. Inclusion of gravity in EBTEL shows better agreement with FH90, but this must be regarded as serendipitous. The EBTEL and FH90 temperature maxima differ by a similar magnitude to that between EBTEL and Hydrad, but there are differences in the decay phase.

Triangular and other profiled heating pulses such as Gaussians also reveal limitations with FH90, as discussed in their Appendix A. The key assumption behind their approach is that the heating function changes "slowly": that is, the timescale is slower than the local conductive cooling time. We find that heating functions which violate this condition give unacceptable answers, including values of the key parameter $\Omega >> 1$ and $< 0$, the former destroying the solution entirely. Thus the method cannot then be used. This is seen in Figure 3, and is a problem even for quite long (500 s) triangular pulses. The spiky behaviour of the density around the time of maximum heating corresponds to extreme values of $\Omega$. The FH90 model thus works only for flat heating profiles, such as the square wave discussed in their paper, and in Figure 2 here.

**4.4 Nanoflares: Gaussian pulse**

To compare with AT09, we need to use a Gaussian temporal heating profile: $Q = Q_0 \exp\left(-\left(t - t_m\right)^2 / 2\tau_H^2\right)$. We do not show KP93 here since its limitations are discussed above. FH90 is also not shown because the pulses considered change too rapidly. Deciding a basis for assessing the AT09 model is non-trivial. They discuss a range of values of the parameter $L/s_H$, where $s_H$ is the scale height of the heating, and positive (negative) values correspond footpoint (apex) heating. There is an abrupt change in the solution when $s_H$ changes sign, even as $L/|s_H| \rightarrow 0$ from both directions. We concentrate on uniform heating and show how the different approximations used for footpoint and apex heating in AT09 apply in the limit of large $|s_H|$.

Fig 4 shows a case with $L$ = 25 Mm and a Gaussian pulse with $\tau_H$ = 40 sec, $t_m$ = 200 sec and a peak amplitude of $10^{-2}$ ergs cm$^{-3}$ s$^{-1}$. The top row shows the apex temperature and density, and the lower one the pressure, and radiative and conductive cooling times for roughly uniform heating. The apex heating (AH) formalism is dotted, the footpoint heating (FH) one dashed, EBTEL and Hydrad are the solid and thick lines respectively, and the AT09 solutions are terminated when they return to the pre-heating state. The AH model gives a higher temperature, density and pressure than the FH one, and has slightly faster cooling. The average AH temperature agrees well with EBTEL up to its maximum value. This can be attributed to the "4/3" factor

introduced by AT09 to ensure that AH agreed with their hydro simulations. The FH model average temperature is lower than EBTEL by the factor of 4/3.

Since the same total energy is going into AH and FH cases, the pressure (lower left) shows a surprising difference between the two models. This requires an understanding of the density behaviour (see below), but implies that the footpoint model has a larger (implied) radiative loss from the loop, especially in the rise phase, than the apex one. This large loss occurs neither in EBTEL nor Hydrad.

The principal feature of these results is the behaviour of the AT09 density. Both AH and FH models have the peak density occur much closer to the time of maximum temperature than EBTEL and Hydrad (50 secs rather than several hundred secs), and the maximum densities are much smaller. The short delay between the temperature and density maxima is due to the assumption in AT09 that the delay is proportional to $\tau_H$. In fact, a reasonable estimate for the delay is that it is proportional to the time taken for material to evaporate due to a downward heat flux from the chromosphere to the corona ~ $L/V$, where $V$ is some fraction of the sound speed based on the coronal temperature: for this example, a few hundred secs.

The consequences of this assumption can be seen in the lower right panel. The peak density should occur at the time when conductive and radiative losses are roughly equal (more precisely, when the TR can radiate away all the downward heat flux: this leads to a factor 2 difference from using purely coronal radiation). The lower right panel show the conductive and radiative cooling times respectively for the two AT09 models and EBTEL. [Note the difference in time ranges compared to the other plots.] To make the comparison with AT09, we use the definitions of cooling times from their paper. The cooling times are equal in both AT09 and EBTEL at around 850 secs. At 240 secs, when AT09 impose their maximum density, their conduction cooling time is shorter than the radiative one by a factor 10. Thus, in this case, the peak density is enforced at a time when conduction-driven evaporation should still be dominant and the density should still be rising. The temperature is also constrained at this time to be half its maximum, which is faster cooling than EBTEL/Hydrad find. The maximum density itself is calculated from a static loop scaling law (i.e. $n \sim T^2$)

under the assumption that the temperature at maximum density is half the maximum temperature. So for this example, the AT09 model seems inappropriate.

We next look at a pulse of longer duration for the AT09 apex heating: the footpoint heating is not considered further. Figure 5 shows a longer pulse ($\tau_H$ = 300 secs) peaking at 2000 secs with the same amplitude heating. Several changes are evident. The temperatures show good agreement at all times. The delay between the AT09 and EBTEL density peaks is reduced to almost zero. However, the discrepancy between the density maxima is similar and the amount of the energy input that appears as thermal energy diminishes. But, for these parameters, AT09 does better.

We have looked at $\tau_H$ in the range 40 – 800 secs, peaking at $t_m$ = 3000 secs, for short (25 Mm) loops. The results are summarised in Figures 6, and similar results are found for nanoflares in long loops. Stars and circles are EBTEL and AT09 results with apex heating. The three diamonds are Hydrad runs. The six panels show the time of the maximum temperature and density <u>after</u> 3000 secs ($t_{m3}$ and $t_{p3}$), the maximum temperature and density, and the ratios $T_{max}/T(n_{max})$, $n_{max}/n(T_{max})$. AT09 predict that $t_m$ is constant, $t_p - t_m$ proportional to $\tau_H$, $T_{max}/T(n_{max})=2$ and $n_{max}/n(T_{max})=2$, and these are what indeed are found for AT09, though the two ratios are slightly lower than 2 due to the presence of background pre-heating plasma as discussed in Appendix B.

The magnitude and timing of the temperature maxima show some differences between EBTEL, Hydrad and AT09, but we do not regard these as especially significant. The delay of $t_m$ in EBTEL can be attributed to the fact that conduction and heating do not quite balance in the rise phase (*dp/dt* needs to be included). The difference between the EBTEL and Hydrad maxima is familiar from Paper 2, and reflects on the approximate nature of the heat flux in EBTEL.

Turning to the density, the EBTEL value of $t_{p3}$ rises slowly from 600 to 800 secs as $\tau_H$ increases, whereas with AT09 $t_{p3}$ increases linearly with $\tau_H$. The Hydrad values of $t_{p3}$ agree well with the EBTEL ones. We argued earlier that the delay of the density maximum should be of order *L/V*, with V some fraction of $C_s$, and should be largely independent of $\tau_H$. For peak temperatures of 5 $10^6$, this is of order a few hundred secs.

It is also clear that the assumptions concerning the temperature and density at their respective maxima in AT09 are not correct. EBTEL and Hydrad show that, while it is reasonable to assume that the pressures at $t_p$ and $t_m$ are equal, the factor "2" relating temperature and density at $t_p$ and $t_m$ is in general incorrect. The consequences are as follows. For small $\tau_H$ the transition to draining occurs when the loop should still be filling up due to conduction-driven evaporation, so giving a low density. For longer pulses, the transition takes place too late.

Thus, for AT09, we draw the following conclusions: (a) the Gaussian formalism for the density at all times and the temperature after its maximum is inappropriate, (b) the relation between the density maximum and its value at maximum temperature is in general invalid and (c) the transition to loop draining is applied at an incorrect time. The reason for this behaviour is the assumed Gaussian density in AT09, and the associated assumptions about the relative timing of the maximum temperature and density. These may be valid over a limited domain of pulse lengths, but in general should not be used. For all pulse lengths, the densities are too small.

### 4.5 Flares

Finally, we looked at these models briefly with flare parameters. FH90 continue to do well for square wave pulses, but have difficulties for profiled ones. KP93 have the same problem with incorrect loop draining. Similar conclusions also hold for AT09. Figure 7 shows the same quantities as Figure 6, except the maximum energy deposited is 2 ergs $cm^{-3}$ $s^{-1}$. The conclusions are as in Section 4.4.

## 5. Discussion

This paper has compared several 0D hydro models for the evolution of coronal loops subjected to impulsive heating. We have outlined the physics needed to model this with reasonable accuracy, and demonstrated, using a number of these models, what happens when this essential physics is omitted. The following discussion can be grouped conveniently around four topics.

### 5.1 Lessons for developing a 0D model

The two main lessons from this study are:

(i) 0D models are best developed from approximate solution of the corresponding 1D equations, making use of fundamental conservation laws. This can lead to solutions that are either continuous or piecewise continuous in time. Empirical models that do not pay attention to these conservation laws (e.g. AT09) are unlikely to succeed.

(ii) Inclusion of TR energetics and dynamics is essential for handling all phases of a coronal heating and cooling cycle. TR radiation governs the mass flow to and from the corona and hence how a loop fills on being heated, and how it cools once the heating is turned off.

A third more minor point worth noting is that some models lead to the "creation" of energy, especially during the initial heating phase. This arises from the neglect of the *dp/dt* term in the energy equation, so that heating must balance conduction at all times. This appears to be a minor problem in FH90. In AT09 it appears to be more significant for short pulses, though the extent is hard to pin down. We do not believe that this influences the subsequent evolution of the loop in a major way.

### 5.2 Comparison of archival 0D models with 1D models

The older 0D models claimed good agreement when compared with 1D hydro simulations: KP93 and FH90 with Pallavicini et al (1983: P83) and AT09 with T04. We have looked at these comparisons to assess why subsequent disagreement occurs.

(i) KP93 compared the pressure and temperature with a square wave heating simulation of P83 (Figure 1 of KP93 and Figure 7 of P83). EBTEL agrees quite well with both up to the peak temperature, but then KP93 and P83 see a much faster decrease in T and p. The P83 density (not shown by KP93) has better agreement with EBTEL, but the maximum still appears to be a factor two smaller.

(ii) FH90 likewise compared their results with a square wave simulation from P83, but for a more intense flare (Figures 5 and 6 of FH90 and Figures 9 and 12 of P83). P83 show faster cooling than FH90, but the agreement between FH90 and P83 is better than between KP93 and P83. However, FH90 did not show a comparison of the density, and Fig 9 of P83 clearly shows a density increase after the heating is terminated, something ruled out in FH90.

(iii) AT09 claim agreement with the 1D hydro simulations of T04, but we note that the 1D hydro simulations were used extensively to parameterise the AT09 model. The agreement between peak temperatures in AT09, EBTEL and Hydrad is positive. However, it is disturbing that AT09 (and by implication T04) have such persistent and large density discrepancies with EBTEL and Hydrad.

We believe a major reason for low densities in some 1D hydro models is numerical under-resolution of the TR. Using the Hydrad code we have recently demonstrated (Bradshaw and Cargill, 2012) that such under-resolution in an impulsively heated loop has little effect on the peak temperature, while changing the peak density by factors of 2 to 8, depending on the lack of resolution. Also, an adaptive mesh is necessary since the TR moves in response to heating so that even innovative (but fixed) grids such as in P83 will have difficulties. A further problem with T04 appears to be the rather shallow chromosphere attached to the base of the loops. We believe that the AT09 model is parameterised on the basis of incorrect 1D modelling.

**5.3 What 0D models don't do and does it matter?**

(i) Change of loop length in response to heating. The result of impulsive heating is to push the top of the chromosphere downwards. This leads effectively to a longer loop whose magnitude has been estimated as $dz = \lambda \ln((\gamma - 1)E / p_0)$: Klimchuk, (2006) where $\lambda$ is the chromospheric scale height, $p_0$ the initial pressure at the top of the chromosphere and $E$ is the total energy deposited in the loop. For a chromosphere with a temperature of 30 kK, as used in Hydrad, $\lambda = 1.8\ 10^8$ cm. For the cases discussed in Figures 2 and 3, $dz/\lambda \sim 3$, or $dz/L \sim 0.2L$ *(*$0.067L$*)* at the end of the heating phase for short (long) loops. These values are larger for flaring cases. This

should lead to 0D models over-estimating the coronal density since pushing the chromosphere downwards requires that the evaporated plasma fit into a larger volume. However, the time of maximum density is not the same as the time of maximum pressure (see Figures), with the pressure decreasing by 20 – 30% in that interval so that *dz/L* will be somewhat smaller. All of this suggests that the density from 0D models will be 10 – 20% above corresponding 1D ones. However, we have included this modification to the length in EBTEL and find that while the peak density does decrease, it is by much less than predicted above, under 10%. This is because, as the length increases, other effects also come into play.

(ii) Neglect of high-speed flows. All 0D models neglect terms proportional to $V^2$ in the momentum equation. EBTEL defines the velocity as being evaluated at the base of the corona. We have calculated a posteriori the Mach number there. For nanoflares neglect of these terms is justified. For larger energy releases, the neglected terms are potentially important during the rise phase of the flare. Immediately after the heating is turned on, when the temperature is still small and sound speed low, the Mach numbers are large but as the temperature rises rapidly, the sound speed increases and the Mach number falls back. By the time maximum temperature and subsequently maximum density are reached, the neglected terms are small.

In fact, these a posteriori velocity calculations will not reflect reality. We know from Hydrad that up to nearly the time of maximum temperature, almost all the energy deposited in the loop is transferred to thermal energy. So any "missing" kinetic energy must be at the expense of that thermal energy which suggests that the upflows are in reality limited to some fraction of the sound speed: an analogous argument was invoked to limit the magnitude of evaporative upflows in flares in response to thick target electron beam heating to of order the sound speed (Fisher et al., 1984; Fisher, 1987). The consequences are that the loop will, during this first phase, fill slightly more slowly than calculated by EBTEL. However, the major part of the density increase occurs close to and after the temperature maximum, during a phase of subsonic evaporation, so the delay should not be large.

### 5.4 Final remarks on 0D models

To conclude this series of papers, we return to Table 1. It can be seen over the last 2 decades how a workable 0D model was developed. FH90 and KP93 identified methods to handle evaporation in response to thermal conduction, KP93 being the more pleasing since evaporation in the absence of heating was included. FH90 and C94 realised how to incorporate radiative cooling in a way that gave rise to over-dense loops. Papers 1 and 2 showed how the TR can respond correctly to conductive and enthalpy fluxes while incorporating the other important effects. It is essential to include the correct TR physics in 0D models. Despite being thin, its radiative loss in equilibrium loops is twice that of the corona, so that the TR tail wags the coronal dog.

What future developments can be expected from such models? The work described in Papers 1 and 2 does rely on a set of constants (or parameters) whose values must be determined by other means such as simulations or equilibrium models. Improvements certainly are possible there though care must be taken that such parameterisations make good physical sense: this paper has demonstrated what can happen when this does not happen. We noted in Paper 2 that systematic differences of 10 – 20% could occur between EBTEL and a 1D benchmark. Is this something to worry about? Perhaps not, given the accuracy of current observations, but also because removing such discrepancies will involve developing more complex 0D models with harder-to-understand parameterisations. And the whole point of 0D models is that they be simple, subject to certain basic principles of how the corona works, as discussed in this series of papers.

**Acknowledgements**

J.A.K. and S.J.B acknowledge support from the NASA SR&T program. We are grateful to the International Space Science Institute (ISSI) for supporting our team, and to Helen Mason for acting as co-leader of this team with SJB.

**Appendix A: Fisher and Hawley Model**

Rather than working in terms of a density, Fisher and Hawley (1990: FH90) use the column depth $N(s) = \int_0^s n(z)dz$ as a variable, and define the total mass per unit area at any time as $N_t = \int_0^L n(z)dz$. We can recover the density by writing $n(t) \approx C_N N_t(t)/L$ where $C_N$ is a constant defined by Eq (12) of FH90. They write Eq (4) in the form:

$$\frac{1}{\gamma - 1}\frac{d\overline{p}}{dt} = \overline{Q} - \overline{R} \qquad \text{(A1)}$$

assuming symmetry at the apex and vanishing heat and enthalpy flux at the base. Here $\overline{Q}$ and $\overline{R}$ are averages per unit volume.

They assume that loop evolution can be split into three phases depending on the ratio of the heating to radiation terms in (A1). These are: (i) strong evaporation when $\overline{R} < \overline{Q}/2$, (ii) strong condensation when $\overline{R} > 2\overline{Q}$ and (iii) quasi-equilibrium at other times. The factors ½ and 2 in (i) and (ii) are arbitrary, but in our experience are sensible. In a heating-cooling cycle the sequence should be (i) – (iii) – (ii). The drawback in this approach is that it does not model evaporative cooling in the absence of heating (see also Paper 1), the model defaulting to phase (ii) automatically.

FH90 organise these phases around a relationship between $N_t$ and $p$ of the form:

$$\frac{1}{N_t}\frac{dN_t}{dt} = \Omega\frac{1}{p}\frac{dp}{dt}, \text{ or } N_t \propto p^{\Omega} \text{ or, in terms of n, } n \propto p^{\Omega} \qquad \text{(A2)}$$

Using the ideal gas law, we see that this implies simple scalings between $n$ and $T$ of the form $T \sim n^{(1-\Omega)/\Omega}$. $\Omega$ = 2/3 gives the static loop scaling law, $\Omega$ = 1/3 the radiative cooling scaling law $T \sim n^2$ and $\Omega >> 1$ gives constant-pressure evaporative cooling. FH90 use only the first two of these.

To evaluate the radiative losses, for a given column density and temperature FH90 use the equivalent losses from an equilibrium loop <u>including</u> the TR. We note that radiative losses are sometimes weak in phase (i) but do matter in phase (ii), and also

believe that equilibrium losses overestimate the real losses in phase (ii) (Paper 2, Bradshaw and Cargill, 2010b). FH90 rewrite Eq (A1) using (A2) to obtain:

$$\frac{1}{\gamma-1}\frac{dN_t}{dt} = \frac{\Omega N_t}{p}\left[\overline{Q} - KN_t^{\lambda}\right] \tag{A3}$$

where $K$ and $\lambda$ are defined in FH90, Eq (13). One can substitute $nL$ for $N$ in (A3) if desired. We do not reproduce the analysis of FH90 for phases (ii) and (iii) because the outcome is not at variance with the work of others. In phase (iii) they set $\Omega = 2/3$, and solve (A3) with (A2) subject to initial conditions obtained at the transition from phase (i). For phase (ii) the authors argue that $\Omega < 0.46$ for $\alpha = -2/3$, the power-law index of the radiative loss function. This gives *T-n* scalings consistent with our present knowledge of this phase in the absence of stratification (Bradshaw and Cargill, 2010a,b). We set $\Omega = 0.33$ since this corresponds to the "default" radiative scaling used in Paper 2.

In phase (i) FH90 derive a conductive cooling model with similarities to that of the Antiochos and Sturrock (1978), with a balance between downward conduction and upward enthalpy fluxes. Integrating the energy equation twice over the loop and applying boundary conditions gives:

$$\frac{1}{N}\frac{dN}{dt} = \frac{\varsigma}{p}\frac{\kappa_0 T_A^{7/2}}{L^2} \tag{A4}$$

where $\zeta = 0.2913$ and $T_A$ is the apex temperature. [The factor $\zeta$ is almost identical to the factor 2/7 = 0.2857 that arises from a simple approximation to the heat flux.] For constant pressure along the loop, the equation of state gives:

$$T_A(t) = T_{A0}\left(1 + t/\tau_{c0}\right)^{-2/7} \tag{A5}$$

where $\tau_{c0} = 2pL^2/\left(7\varsigma\kappa_0 T_{A0}^{7/2}\right)$ is the conductive cooling time at $t = 0$. This can be compared with the solution of Antiochos and Sturrock (see Cargill, 1994, Eq 8 and 9) which has $\tau_{c0} = 5p(L/1.6)^2/\left(2\kappa_0 T_{A0}^{7/2}\right)$. The numerical coefficients are the same to 1%. Enforcement of the boundary conditions then leads to an expression for the pressure as a function of $T_A$ and $N_t$: $p = 2^{2/3}\eta 2kT_A N_t/L$ where $\eta = 0.4656$. This in turn determines the apex density in terms of $N_t$ as $n_A = 2^{2/3}\eta N_t/L = 0.74N_t/L$, in contrast with $n_A = 0.78N_t/L$ during phase (iii): FH90, Eq (12).

This solution, which describes evaporative, conduction-driven cooling in the absence of heating (a phase not actually modelled by FH90), is then modified to account for heating, and to permit use of the Ω formalism. FH90 determine $T_A$ by balancing conduction and heating:

$$T_A = \left( \frac{(\gamma - 1) Q L^2}{\varsigma \kappa_0} \right)^{2/7} \tag{A6}$$

and then derive an expression for Ω in this phase:

$$\Omega = \left( 1 + \tau_c \frac{d \ln(Q)}{dt} \right) \tag{A7}$$

where $\tau_c$ is just the previous conductive cooling time defined now for all times. The solution is obtained by solving (A2) and (A7) for $N_t$ and then calculating $T_A$ and $p$ as described above. We have been able to reproduce successfully the results shown in Figure 5 of FH90 which involves a square wave heating function, so that Ω = 1. For their Figure 6, we find a change from evaporative cooling to quasi-equilibrium at 250 secs, which is different from FH90. Their results can be reproduced by changing the condition for strong evaporation to $\overline{R} < 0.62\overline{Q}$. We do not regard this discrepancy as especially significant.

**Appendix B. Aschwanden and Tsiklauri (AT09) model**

Although AT09 has similar aspects to parts of other models, in general it approaches the problem differently, relying on empirical specifications based on the numerical work of T04. AT09 use a Gaussian heating function of the form $Q = Q_0 \exp\left(-(t-t_m)^2 / 2\tau_H^2\right)$ and can include a spatial dependence of the heating function, obtained by multiplying $Q$ by $\exp(-s/s_H)$ to give apex or footpoint heating depending on the sign of $s_H$ and the location of the origin. We neglect the spatial structure of the heating function but note that parts of the AT09 model differ by numerical factors depending on whether $s_H$ is positive or negative as $|s_H| \to \infty$.

AT09 consider three phases: (i) heating up to the temperature maximum at time $t_m$, (ii) from then until the density maximum at time $t_p$ and (iii) the final cooling. In phase (i), AT09 assume a balance between heating and conduction. We are not concerned here with the spatial temperature structure, and the apex temperature is given by:

$$T_a(t) = \left( \frac{7L^2 Q_0}{4\kappa_0} \exp\left( -\frac{(t-t_m)^2}{2\tau_H^2} \right) \right)^{2/7} \qquad \text{(B1)}$$

For apex heating, this is multiplied by a factor 4/3 to agree with simulations of T04.

Calculation of the density is empirical, relying on the T04 simulation results. AT09 set $n_p = n(t=t_p) = 2n_m = 2n(t=t_m)$, assume $p(t_p) = p(t_m)$, so $T_p = T(t=t_p) = 0.5T_m$. This leads in turn to $t_p = t_m + \tau_H \sqrt{7\ln(2)}$. The density for $t < t_p$ is given by:

$$n_a(t) = n_p \exp\left( -\frac{(t-t_p)}{2\tau_{evap}^2} \right) \text{ where } \tau_{evap} = \frac{(t_p - t_m)}{\sqrt{2\ln(2)}} \qquad \text{(B2)}$$

To calculate $n_p$, AT09 use a modified static loop scaling law, but include various factors to obtain agreement with T04. For uniform heating, we have $p(t=t_p)L = \left(T(t_p)/1400\right)^3 q$, $q = 1 - \exp(-\tau_H / \tau_{fill})$, and $\tau_{fill} = L / c_s(T = T(t_p))$. For apex heating the expression for $p$ is multiplied by 0.7 and for footpoint heating other numerical factors are included. Calculation of $T$ and $n$ at maximum density from such a scaling law is reasonable since it is equivalent to conductive and radiative cooling being approximately equal. The role of the factor $q$ is unclear. Clearly it fails

in the limit of small pulses when significant density enhancements are obtained and the peak density corresponds to a time of equal conductive and radiative losses. Also, this formalism for $n_p$ ignores the physical nature of the interaction of corona, TR and chromosphere, except through some parameters to obtain agreement with T04. The consequences of this are shown in Section 4.4.

For times after $t_p$, AT09 calculate the cooling using the parametric fit:

$$T(t) = T_p\left[1 - \frac{(t - t_p)}{n_{cool}\tau_{cool}}\right]^2 \text{ where } \frac{1}{\tau_{cool}} = \frac{1}{\tau_c} + \frac{1}{\tau_r} \qquad \text{(B3)}$$

and $n_{cool}$ is chosen as 4 from the apex simulations of T04. The density in this phase follows the $T \sim n^2$ scaling, valid only for purely radiative cooling. The inclusion of conduction will tend to increase the coefficient in the *T*-*n* power law. Doubtless the various parameterizations take this into account.

We have used the original SolarSoft version of the AT09 model, and calibrated our version of it against Figure 7 in AT09. Noting that *L* in this Figure is the total loop length, we need to include a background heating of roughly 5 $10^{-4}$ ergs $cm^{-3}$ $s^{-1}$ to recover their results. Since the initial (pre-flare) temperature and density do not arise in AT09, it is of interest how this included. In the SolarSoft version of AT09 used to obtain their results:

$$T_* = T_B + T(1 - T_B / T(t = t_m)),\ n_* = n_B + n(1 - n_B / n(t = t_p)) \qquad \text{(B4)}$$

Here "*" denotes the value plotted (and tabulated) in AT09, "B" the background quantity and un-subscripted the value calculated from the AT09 model. For a large energy release this approximation makes little difference. For smaller heating events, one can question whether a linear superposition is optimal.

**Table 1**

| Model | Pre-event state | T-rise | Evap | Radn | Gravity | Heating (t) | Heating (s) | Energy Conserve |
|---|---|---|---|---|---|---|---|---|
| FH90 | Y | Y[2] | N | Y | N | Restricted[8] | N | N |
| KP93 | Y | Y | Y | N | N[6] | General | N | Y |
| C94 | Y | N[3] | Y[3] | Y | N | Instantaneous | N | Y |
| EBTEL | Y | Y | Y | Y | Y | General | N | Y |
| AT09 | Y[1] | Y[2] | Y[4] | Y[5] | Y[7] | Gaussian only | Y Exponential | N |

Table 1. The successes of the various models. The columns show: (1) The model. (2) Pre-event state: is a background *T* and *n* prior to heating included? (3) *T*-rise: is the initial heating up to maximum temperature included? (4) Evaporation: does the loop density increase in response to a heat flux after maximum temperature and in the absence of heating? (5) Radiation: is the radiative cooling phase modelled correctly? (6) Gravity: is stratification included? (7/8) Heating(*t*,*s*): any possible temporal and spatial profile of heating function. (9) Energy conserve: Is energy conservation guaranteed? "Y" means success, "N" means it is not guaranteed to handle this aspect properly (Section 5.1). The notes below discuss caveats to the conclusions:

1. Not discussed in Paper. Included in original SolarSoft code and is required to reproduce results in AT09.
2. Neglects *dp/dt* term. Instantaneous balance between conduction and heating. Leads to possible violation of energy conservation in this phase
3. Instantaneous rise to maximum temperature.
4. Density does increase, but not modelled correctly.
5. Transition to radiative cooling occurs at wrong time.
6. Only included in plasma draining model
7. Maximum density calculation only. Footpoint heating only.
8. Needs to be very slowly varying.

**References**


Antiochos, S. K., 1980, ApJ, 241, 385

Antiochos, S. K., Sturrock, P.A. 1978, ApJ, 220, 1137

Aschwanden, M. J., & Tsiklauri, D. ApJ Supp, 185, 171

Bradshaw, S. J., & Mason, H. E. 2003, A&A, 401, 699

Bradshaw, S. J., & Cargill, P. J. 2006, A&A, 458, 987

Bradshaw, S. J., & Cargill, P. J. 2010a, ApJ Lett., 710, L39

Bradshaw, S. J., & Cargill, P. J. 2010b, ApJ, 717, 163

Cargill, P. J. 1994, ApJ 422, 381

Cargill, P. J., Mariska, J. T., & Antiochos, S. K., 1995, ApJ, 439, 1034

Cargill, P. J., Bradshaw, S. J. & Klimchuk, J. A., 2012, ApJ, 752, 161

Hansteen, V. H. 1993, ApJ, 402, 741

Fisher, G. H., Canfield, R. C. & McClymont, A. N., 1984, ApJ Lett., 281, L79.

Fisher, G. H., 1987, ApJ, 317, 502.

Fisher, G. H., & Hawley, S. L. 1990, ApJ, 357, 243

Hansteen, V. H. 1993, ApJ, 402, 741

Klimchuk, J. A., 2006, Solar Phys., 234, 41

Klimchuk, J. A., Antiochos, S. K., & Mariska, J. T. 1987, ApJ, 320, 409

Klimchuk, J. A., Patsourakos, S., & Cargill, P. J., 2008, ApJ, 682, 1351

Kopp, R. A., & Poletto, G. 1993, ApJ, 418, 496

Kuin, N. P. M., & Martens, P. C. H. 1982, A&A, 108, L1

Mariska, J. T., Doschek, G. A., Boris, J. P., Oran, E. S., & Young, T. R., Jr., 1982, ApJ., 255, 783

McClymont, A. N., & Canfield, R. C., 1983, ApJ 265, 483

Pallavicini, R., Peres, G., Serio, S., Vaiana, G., Acton, L., Leibacher, J., & Rosner, R., 1983, ApJ., 270, 270

Peres, G., 2000, Solar Phys., 193, 33

Serio, S., Reale, F., Jakimiec, J., Sylwester, B., & Sylwester, J. 1991, A&A, 241, 197

Tsiklauri, D., Aschwanden, M. J., Nakariakov, V. M. & Arber, T. D., 2004, A&A, 419, 1149

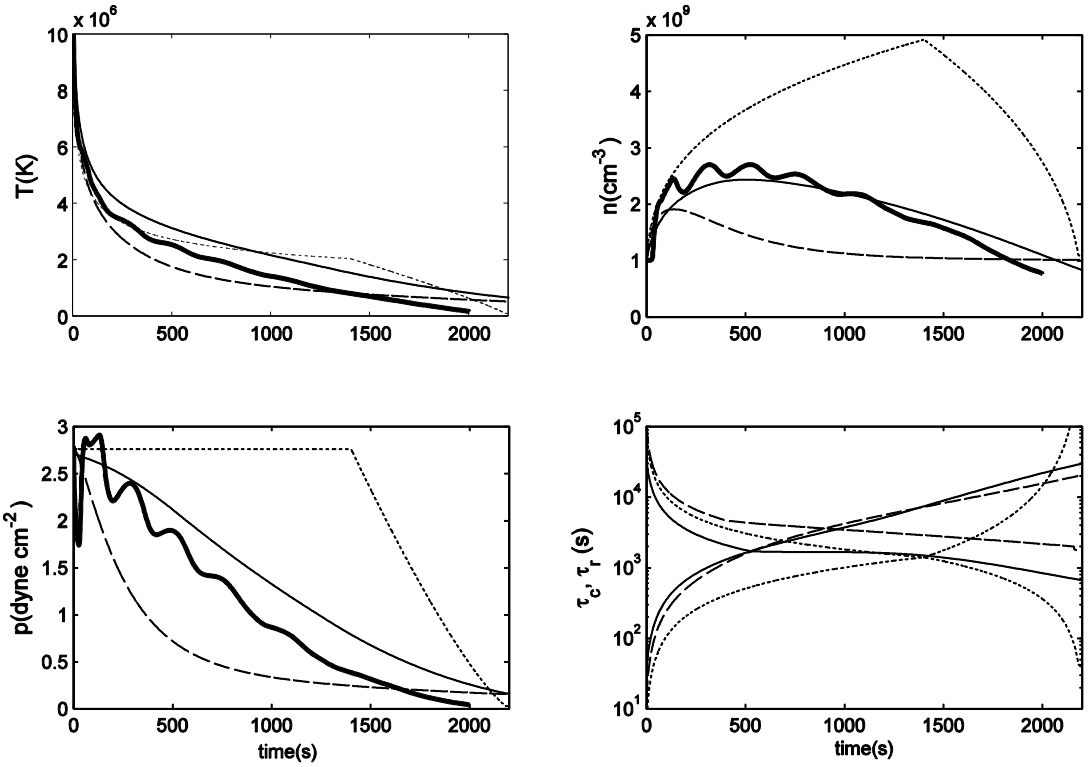


**Figure 1**. Loop cooling showing the models of C94 (dots), KP93 (dashed), EBTEL (solid) and Hydrad (thick solid). The initial temperature and density are $10^7$ K and $10^9$ $cm^{-3}$ and the loop half-length 25 Mm. The four panels show apex temperature and density (top), pressure (bottom left) and conductive and radiative cooling times (bottom right). The conductive (radiative) cooling time is small (large) near $t = 0$.

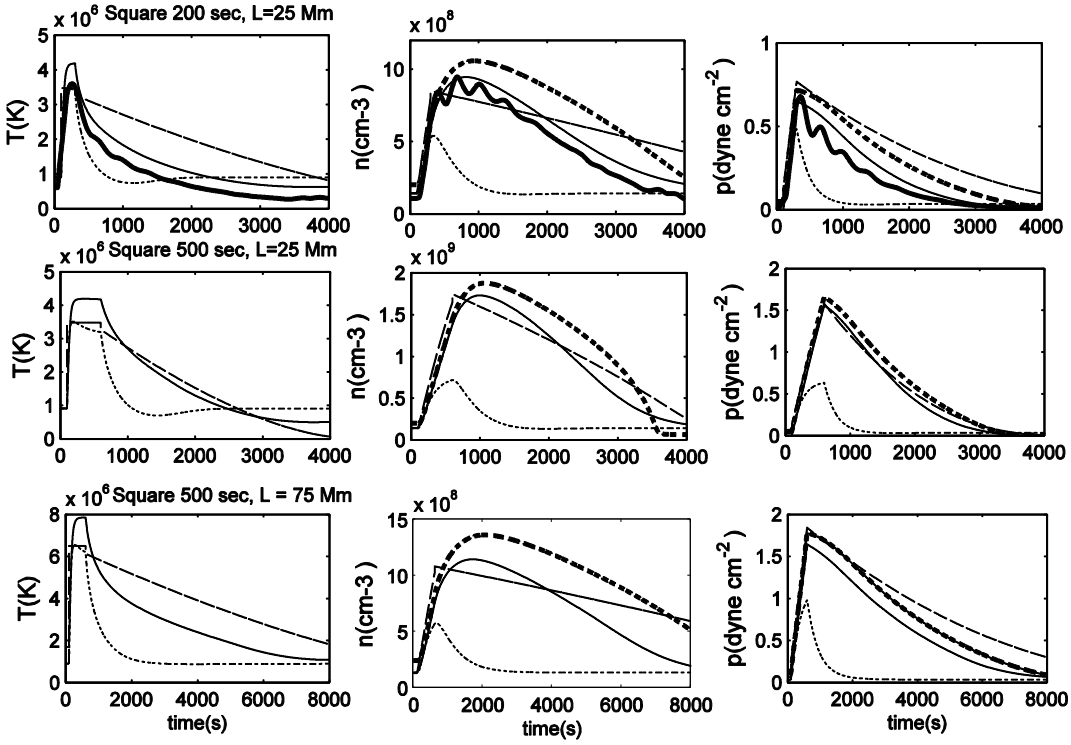


**Figure 2** Nanoflare energy release with a square heating pulse. The three columns show apex temperature, density and pressure as a function of time. The three rows show, from top to bottom, a short (200 s) and long (500 s) pulse in a loop with half-length 25 Mm and a long (500 s) pulse in loop with half-length 75 Mm. The maximum heating amplitude is 5 $10^{-3}$ ergs $cm^{-3}$ $s^{-1}$. The line coding is solid (EBTEL), dotted (KP93), dashed (FH90), thick solid (Hydrad: upper three panels only), thick dotted EBTEL with no gravity and a single power law loss function.

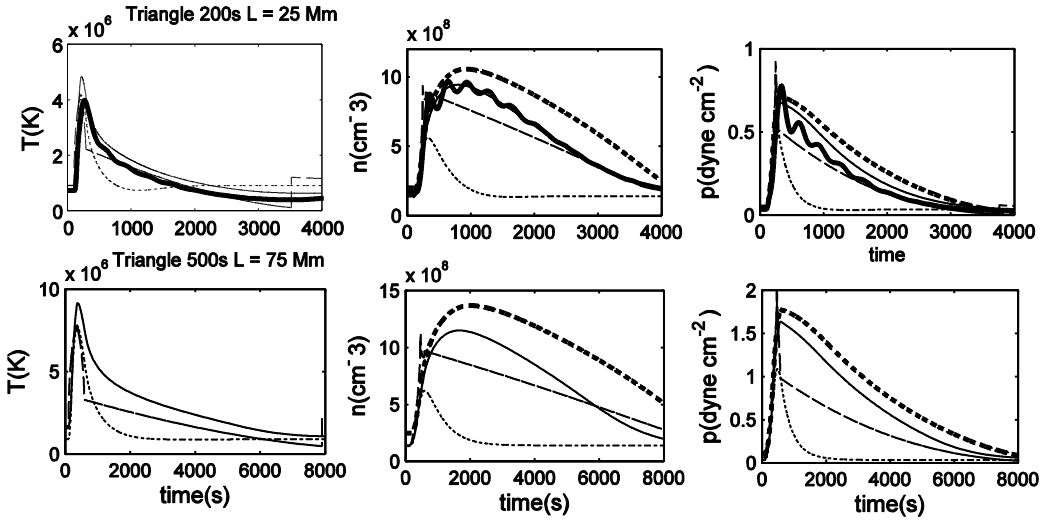


**Figure 3** As Figure 2 except a triangular heating pulse is used. The two rows are a short (200 s) and long (500s) pulse in loops with half-lengths of 25 and 75 Mm. The maximum heating amplitude is $10^{-2}$ ergs $cm^{-3}$ $s^{-1}$.

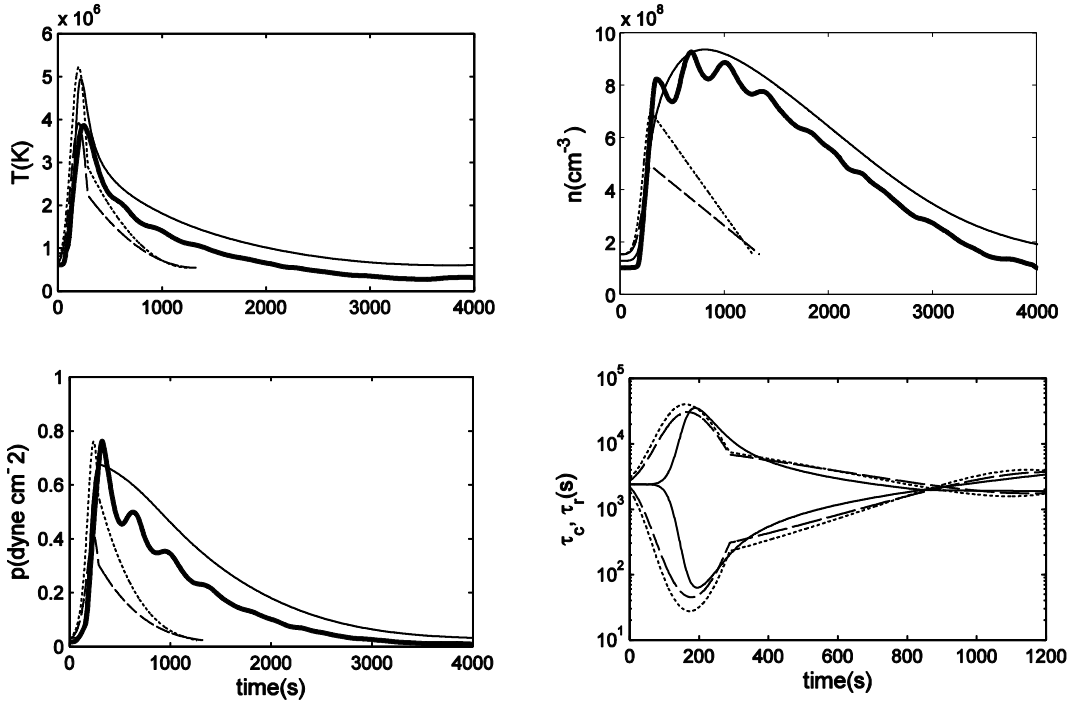


**Figure 4.** Results for a Gaussian heating pulse of width 40 sec, peaking at 200 secs. The dashed (dotted) curve is from AT09 footpoint (apex) heating formalism, EBTEL is the solid line and Hydrad the thick one. The loop has a half-length of 25 Mm and a heating pulse with maximum amplitude $10^{-2}$ ergs $cm^{-3}$ $s^{-1}$.

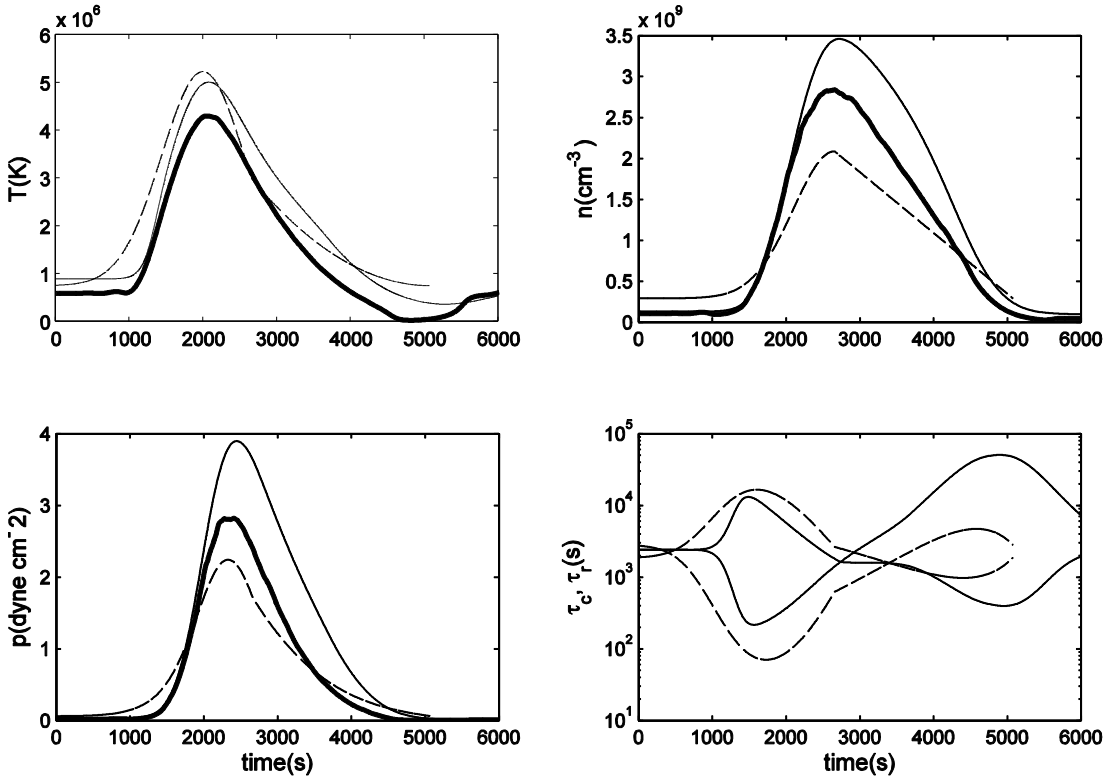


**Figure 5**. As Figure 5, except pulse has width 300 sec and peaks at 2000 secs.

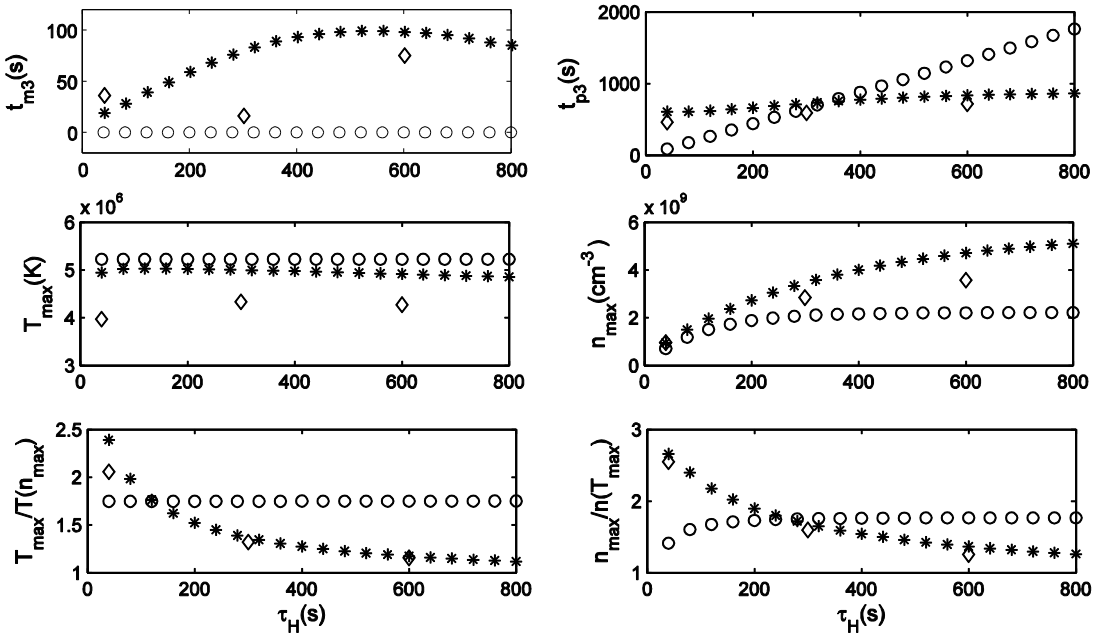


**Figure 6**. Summary of Gaussian heating for a loop with half-length 25 Mm. The horizontal axis shows the pulse width ($\tau_H$). The panels show: the time of maximum temperature and density after 3000 secs, $t_{m3}$ and $t_{p3}$ (top row), the maximum temperature and density (middle row), and the ratios $T_{max}/T(n_{max})$ and $n_{max}/n(T_{max})$ (lower row). Stars denote EBTEL results, circles AT09 with the apex heating model adapted for uniform heating, and the three diamonds are Hydrad runs.

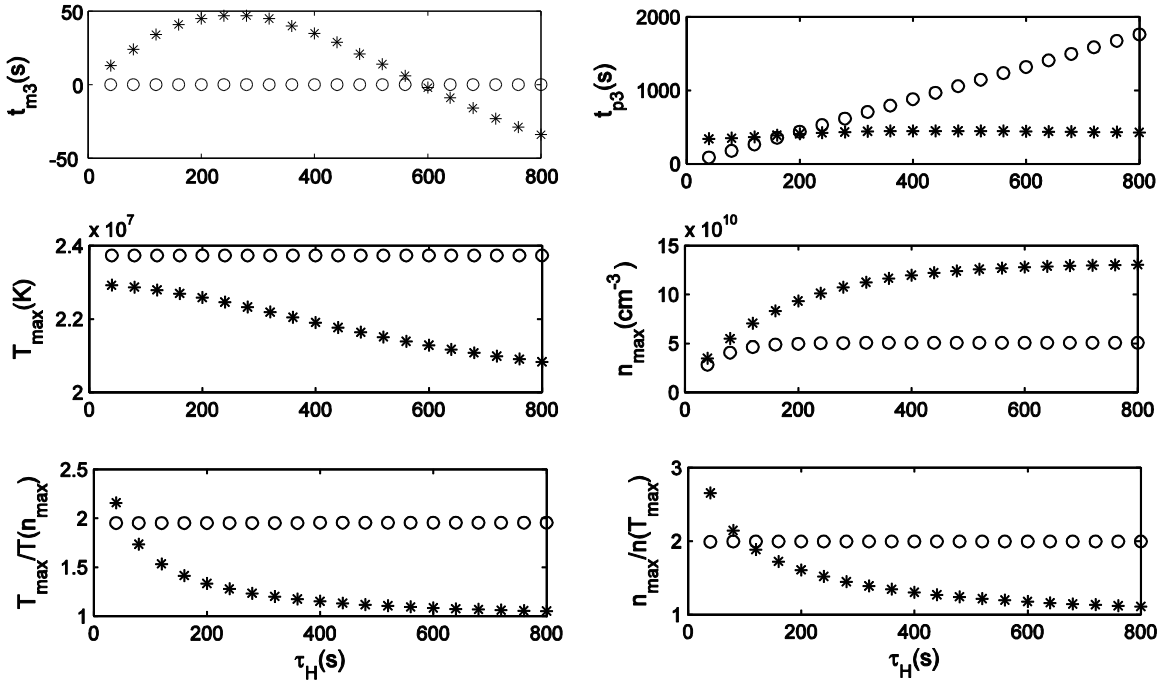


**Figure 7**. As Figure 6, except for a flare case with a maximum energy deposition of 2 ergs cm$^{-3}$ s$^{-1}$.